IEEE Access
Multidisciplinary | Rapid Review | Open Access Journal

Received August 11, 2020, accepted August 26, 2020, date of publication August 31, 2020, date of current version September 11, 2020.

Digital Object Identifier 10.1109/ACCESS.2020.3020455

"Grid"-Less Power Systems: A Vision for Future Structure of Power Networks

MEGHDAD FAZELI[1], (Senior Member, IEEE), PAUL M. HOLLAND[2], (Member, IEEE), AND MUFTAU BARUWA[2]

[1]Energy Safety Research Institute, Swansea University, Swansea SA1 8EN, U.K.
[2]Electrical Engineering Department, Swansea University, Swansea SA1 8EN, U.K.

Corresponding author: Meghdad Fazeli (m.fazeli@swansea.ac.uk)

This work was supported in part by the European Regional Development Fund, through the Welsh Government, through the Flexible Integrated Energy Systems (FLEXIS) Project under Grant 80835.

ABSTRACT This paper proposes a new paradigm in the structure of power systems to facilitate the large scale move to renewables-based distributed generation necessary to help decarbonize the current electricity networks. Since the design of the incumbent power system topologies is to control large synchronous generators, critical control metrics degrade as the penetration of converter-based units increases. Specifically, the reduction in short circuit level, phase angle movement, and rate of change of frequency limit the wider adoption of converter-based units. This paper proposes structural changes and control that inherently solve such critical performance issues through physically decoupling all synchronous generators from the network. A set of back-to-back AC/DC/AC converters controlled by a universal virtual synchronous machine-based control algorithm, introduced in the paper, allows the repurposing of existing plant to enable the integration of more converter-based units. Despite being physically disconnected, this new structure/control still benefits from inertial capacities of synchronous generators to suppress the oscillations caused by disturbances. Moreover, the method enables further exploitation of synchronous generators as energy storage mechanisms. PSCAD/EMTDC simulations demonstrate the advantages of the proposed structure and control system in different normal and abnormal scenarios.

INDEX TERMS Power systems structure, universal control, renewable energy, virtual synchronous machine.

I. INTRODUCTION

In classic power systems theory, a "grid", which consists of hundreds of synchronous generators (SGs), is such an extensive system that the dynamics of one unit "will cause virtually no change in the voltage and frequency" of the network [1]. "Such a voltage source of constant voltage and constant frequency is referred to as an infinite bus" [1] (therefore, in power systems literature/research, the terms "grid" and "infinite bus" are used interchangeably).

Integration of renewable sources led to the creation of distributed energy resources (DERs) [2] and energy prosumers (producers + consumers), which implies that the generation of energy can happen at the so-called transmission, distribution and consumption levels. The intermittent nature of renewable sources necessitates the integration of more energy storage (ES) systems and adaptation of more advanced control/management methodologies to balance the generation and demand, and provide ancillary services e.g. [3]–[6].

For several decades, the well-known dynamics of SGs dominated the power systems operation/control. DERs are decoupled from the network through power electronic converters (PECs), that perform power conditioning, e.g. maximum power point tracking (MPPT). Currently, most PECs are controlled in "grid-following" mode, where the grid imposes the voltage and frequency, and the DERs feed a certain amount of power into the network [7]. Therefore, as the penetration of converter-based systems (CBSs) increases, the number of SGs (that forms the "grid") will reduce. As such, the concept of the "infinite bus" will become dated with less distinction between islanded and grid-connected operation modes. Such a high penetration of CBSs has, therefore, created several challenges for the network operators to maintain system stability. Hence, despite the environmental necessity of using more renewable energy, there are calls/regulations worldwide on limiting it. For example, currently, there is a 65% limit on CBSs in the Irish network [8]. Also, after the massive blackout in the British network

The associate editor coordinating the review of this manuscript and approving it for publication was Yonghao Gui.

(in August 2019), the former director of GB National Grid called for limiting renewables [9].

Mitigating the technical challenges caused by further integration of CBSs, necessitates the utilization of stability provider technologies. Recently, for example, the British National Grid in the ''Technical Performance and Assessment Criteria'' document (downloadable from the ''stability pathfinder'' webpage [10][1]) described the essential and the desirable requirements for a stability provider product. The main requirements are summarized and discussed below:

Inertia: The natural coupling of SGs with the network inherently provides inertia to the system, which is necessary to suppress the oscillations caused by disturbances (such as short circuits and sudden changes of load/generation) [11], [12]. Because of the ''grid-following'' control, CBSs do not contribute to the system inertia even if they have a rotating mass [8], [13]. Hence, as the penetration of CBSs increases, there is a correlated reduction in the system inertia, increasing the risk of instability. There are several calls worldwide to address the reduction in the inertia, e.g. the ''Network Code on Operational Security'' by ENSTO-E (European electricity organization) [14] and the ''stability pathfinder'' program by the British National Grid [10]. A plethora of control algorithms have been proposed in the literature to alleviate the reduction in inertia, e.g. [12], [15]–[20] to name a few. Although different names such as the virtual synchronous machine (VSM) or synthetic/virtual inertia are coined, the common idea is to make the DERs behave like SGs through making their interfacing PECs mimic the dynamics of an SG. Using synchronous condenser (SC)-based solutions to mitigate the inertia drop is also proposed in the literature [21]. British National Grid in [10][1] sets a minimum inertial response of 1.5 pu, while the highest score (in the tender process) will be awarded to the solutions with more than 5 pu inertial contribution.

Short Circuit Level (SCL): While SGs supply a fault current of 5-7 pu, fault current contribution of a CBS is normally about 1.1-1.2 pu. This difference between the SCL contribution may disrupt the operation of the overcurrent protection systems since the fault level will change with different generation portfolios [22]. For example, in a day with a high penetration of DERs the overcurrent relays, because of their inverse-time characteristics, may operate with much longer delay or may not even function. Therefore, the minimum requirement set by GB National Grid is 1.5 pu SCL contribution, while the highest score (in the tender process) will be awarded to the solutions with more than 5 pu SCL contribution.

Transient phase angle change: In SGs, the rotor angle is also the phase angle between the excitation voltage and the terminal voltage. Since rotor angle cannot change quickly, sudden changes of voltage phase angle can trip SGs. The issue becomes more problematic during re-connecting two parts of the system, where care must be taken to make sure that the two sections are fully in phase. British National Grid expects a solution to ''respond up to its rating with reactive current countering the initial voltage angle change'' during and for 0.5s after fault clearance [10][1]. It also expects that solutions ride-through voltage angle deviations of at least 90 degrees within 60ms and up to 200 degrees within 5ms [10][1].

Rate of Change of Frequency (RoCoF): As inertia drops, RoCoF increases. Therefore, a generation/load loss may lead to the RoCoF exceeding the settings of RoCoF-based protection, which would result in unnecessary loss of DERs, and can lead to further disturbances [11]. Recently British National Grid increased the RoCoF threshold from 0.125 Hz/s to 1 Hz/s and specified the solutions to withstand RoCoF $\leq$ 1 Hz/s for 500ms [10][1].

Some of these requirements seem contradictory or at least very difficult to achieve with either SC-based solutions or PEC-based solutions. For example, while contributing an SCL of more than 5 pu is not an issue for SC-based solutions, the only way to do so for a PEC-based solution is to choose over-rated switches.[2] This requirement is understandable from a network operator viewpoint since it keeps the SCL almost unchanged; however, it does not appear to be an optimized solution from a researcher viewpoint. Using SCs in effect means substituting SGs with almost the same infrastructure, which can increase the energy price. Moreover, SCs are likely to be fossil-fueled, which undermines integrating more renewable energy in the first place. Using PECs with over-rated switches (assuming technically possible for high powers) is an over-engineered solution that also increases the price.

While phase angle deviation ride-through requirements are not an issue for PEC-based solutions (since PECs can withstand large phase differences), they can be problematic for SC-based solutions. Also, to the best of the authors' knowledge, no previous study demonstrates that injecting a certain amount of reactive current can maintain the voltage angle change within the range that guarantees the uninterrupted operation of SGs. More importantly, there are already low voltage ride-through requirements, where the reactive power injection depends on the voltage level and the duration of the voltage sag [23] (not the phase angle), which might contradict the new requirements.

It is noted that the RoCoF-based protection for DERs is an islanding detection method, which can, theoretically, be further relaxed (as GB National Grid already did) or even removed. However, since in the current network structure, frequency has both electrical (1/one-cycle-time) and mechanical (rotor speed of SGs) meanings, RoCoF depends on the rate of change of the rotor speed. Because of this dependency between the mechanical and electrical frequency, further

[1]Since the ''stability pathfinder'' process is not finalized, it is subject to change. However, it can be used as an indicator of the functionalities that Network Operators might expect from a stability provider technology.

[2]It is also possible to de-load the DERs during normal operation to have enough capacity available for SCL contribution. This approach will, of course, not be appealing to the DERs' owners.

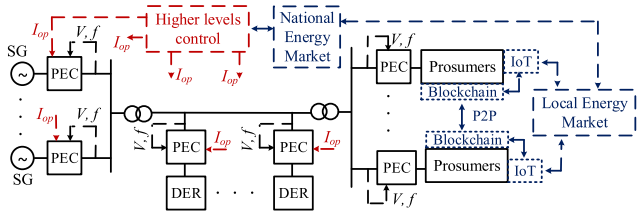

FIGURE 1. A vision for future structure of power systems.

relaxation of RoCoF (and frequency nadir) regulations may endanger SGs operation.

The direct connection of SGs to a network full of PECs can also create unknown issues. For example, [24] claims that the interaction between reactive power controller of wind generators and SGs might generate some new low-frequency oscillatory modes, which can be due to the fundamental differences in the dynamics of SGs and PECs. The popular approach to mitigate this issue is to slow down the dynamics of PECs to match that of an SG. While this approach is understandable for network operators (to maintain the business as usual), it is not an optimized solution. For example, [25] reports that the ability of PECs to "quickly adjust their active and reactive power output could be utilized to mitigate their possible adverse effects on the system".

While the network operators are still struggling in coping with these new conditions, technologies such as Blockchain [26] and Internet of Things (IoT) will soon enable peer-to-peer (P2P) energy trading within neighborhoods [27], which will further complicate electrical energy distribution and control (Fig.1). It seems that in the future most of the energy will be generated by DERs and prosumers who can (or at least have more freedom to) decide from/to whom buy/sell their electricity. In such circumstances, the power system is more like a "network" of lines/cables connecting different units, and the network operators become facilitators and regulators, who create and enforce the standards and regulations. Each segment of such a network should be able to operate independently and supply (critical) loads. Therefore, as shown in Fig.1, future power systems will be analogous to autonomous cars that react to local traffic. I.e. all units (SGs, DERs, prosumers, etc.) should be able to react to the local parameters (voltage and frequency). At the same time, higher-level (secondary and tertiary) controls coordinate the interactions between them (like smart traffic lights).

In light of the above complications, this paper proposes to decouple the SGs from the network by a set of PECs (as shown in Figs.1&2). This paper also proposes controlling all SGs (and all other CBSs) using an updated version of the control algorithm proposed in [28] (see Figs. 2 & 3). The closest network architecture to the proposed structure is presented in [29], where all DERs are connected to the network through VSM-controlled PECs while SGs are still directly connected to the network. However, the architecture proposed in [29] still suffers from all the issues discussed in the previous paragraphs (due to the direct connection of SGs to the network).

It is noted that a "net zero-Carbon" power system does not necessarily mean an SG-free one. For example, nuclear-, hydro- and bio-fueled power plants, which are considered "clean energy" (and renewable for hydro and bio), are SG-based. Therefore, the coexistence of SG-based plants and CBSs is a reality to deal with for decades to come (unless in a 100% wind/solar/tidal-based energy system). The authors believe most (if not all) of these technical challenges result from being in a situation where CBSs interact directly with SGs. For example, the successful operation of a 100% PEC-based microgrid with "zero inertia" was reported in [30]. Similarly, voltage and frequency control of an "inertia-less" islanded microgrid was reported in [31]. Moreover, the use of "inertia-less" VSM was proposed and validated in [32], [33]. Therefore, unlike the popular approach that tries to slow down the dynamics of CBSs to make them behave like SGs, this paper proposes a "steer into the skid" strategy to decouple the SGs from the network by PECs.

The main contributions of the paper are:

- Proposing a new structure for power systems in which all SGs are decoupled from the network by PECs.
- Proposing a new control paradigm for the decoupling PECs (and all CBSs) that still enables full utilization of the inertial capacity of the SGs and further exploits them as ES system.

Using the proposed structure/control will:

- Nullify the reduction in SCL issue through unifying the SCL contribution of all units.
- Protect the SGs against phase angle movements since PECs can easily handle large phase angle changes.
- Enable new RoCoF (and frequency nadir) regulations by separating the mechanical frequency from the electrical frequency.

The other advantages of the proposed structure/control are detailed in the next section.

II. PROPOSED STRUCTURE AND CONTROL METHOD

As illustrated in Figs.1&2, this paper proposes to decouple all SGs from the network by a set of AC/DC/AC PECs, namely: network side converter (NSC) and generator side converter (GSC). This paper also proposes an updated version of the control algorithm in [28], [34] (which is illustrated in Fig.3) to control the NSCs of SGs and other CBSs. All the PECs (NSC, GSC and DERs) are controlled using the classic current-controlled VSC in dq-frame (using PI controllers).

As shown in Fig.3, the control of the SGs' NSCs and other CBSs are very similar in principle and is based on I_d-V_d and I_q-f droops (the only difference is the rotor speed restriction mechanism which is shown in Fig.4 and will be discussed later). The choice of the droop variables is demonstrated in [28], [35]. Since the transferred energy is proportional to the potential difference (voltage), using voltage to regulate active power (rate of change of energy) makes sense (hence I_d-V_d droop). Also, since reactive power is due to the phase difference between voltage and current, using frequency (rate of change of the phase angle) to regulate reactive power makes sense (hence I_q-f droop). The reason that conventionally

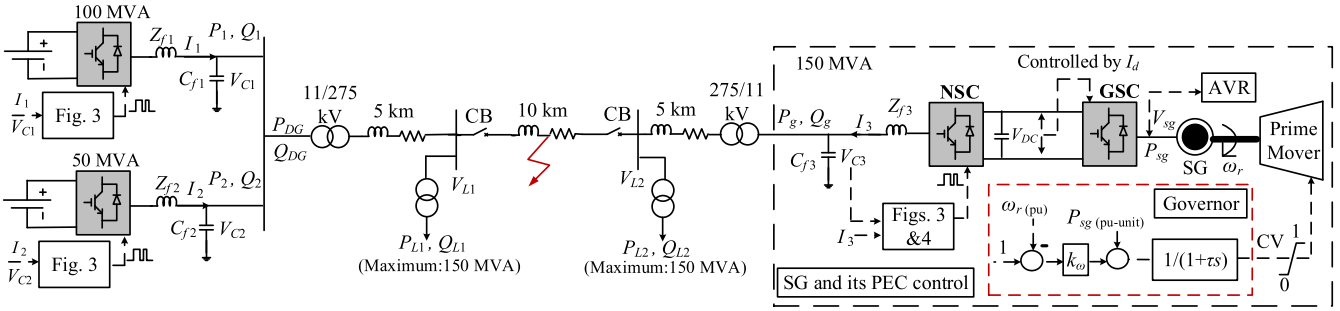

FIGURE 2. The understudy system (for simulation results of sub-section III *A-D*).

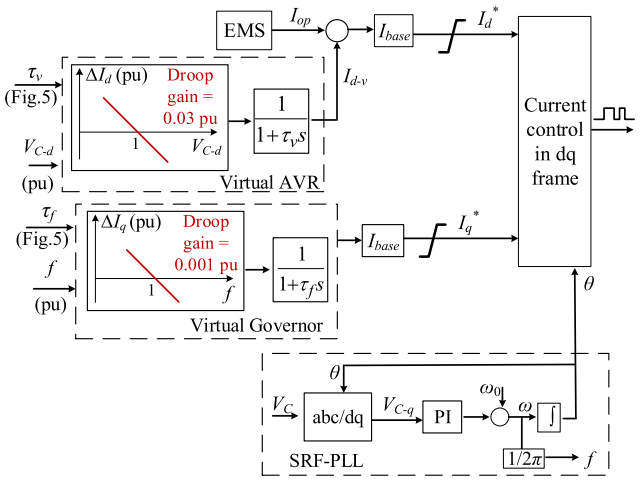

FIGURE 3. Proposed control system for the NSC of SGs and other CBSs.

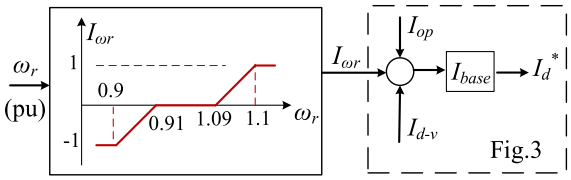

FIGURE 4. Proposed rotor speed restriction mechanism added to the NSC control of SGs (i.e. Fig.3).

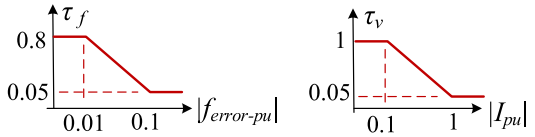

FIGURE 5. Proposed dynamic time-constant selection for the virtual AVR and virtual Governor.

active power and frequency are related is the electromechanical coupling between the SGs and the power system. Due to this coupling, the active power variations will be reflected on the SGs' speed (kinetic energy), which is proportional to the network's frequency. However, since the proposed structure separates the SG from the network, the SGs' speed will no longer affect the network's frequency. Therefore, it is possible to use I_d-V, I_q-f droops for all types of load (see Fig. 6).

To add some dynamics and damping to the system, the outputs of the droops are fed to low-pass filters (LPFs), which represent the virtual automatic voltage regulator (AVR) and the virtual Governor [28]. The output of the virtual Governor is multiplied by the converter's base current I_{base} to set the q-component reference current I_q^*. The summation of the output of the virtual AVR I_{d-v} and the operating current $I_{op}(I_{d-v}+I_{op})$ is multiplied by I_{base} to set the d-component reference current I_d^*. I_{op} is set by the energy management system (EMS). The EMS can be a combination of an MPPT and ES control, for DERs, or a secondary controller (see Fig.1), for SGs/DERs. For example, in [28], where a PV-ES system is considered, the EMS performs both MPPT and ES control. In [34], where wind turbines are studied, the EMS is basically the MPPT.

Since the proposed structure physically decouples the SGs from the network, the SGs' speed must no longer be 50 (or 60) Hz at steady state. The proposed control scheme (Figs. 2 & 3) exploits this situation to enable the SGs operate as ES mechanisms, meaning that their rotor speed can vary. However, there will be a practical limitation for the max/min limits of the rotor speed (e.g. due to the mechanical constrains). To maintain the rotor speed within the limits, the control scheme shown in Fig.4, is added to the NSC control of the SG's (Fig.3). Note that since the rotor speed limitation may vary for different types of SG, this paper assumes a $\pm 10\%$ limit; only to demonstrate the performance of the proposed system (determining the exact speed limitation of different designs of SGs is beyond the scope of this paper). Obviously, a larger/smaller speed limitation, would increase/decrease the ES capacity of the SG. The rotor speed restriction mechanism determines the speed restriction current I_ω according to the rotor speed ω_r (in pu) and add it to the $I_{d-v}+I_{op}$. Assuming a $+/-10\%$ max/min limits on ω_r, I_ω is set as shown in Fig.4. To avoid I_ω jumping between zero and ± 1 pu$_{-\text{unit}}$ (pu$_{-\text{unit}}$ is defined as the pu value based on each unit rating), a $+/-1\%$ is added to the min/max limit. This makes I_ω varies gradually from zero to $+/-1$ pu$_{-\text{unit}}$ for $1.09/0.9 < \omega_r < 1.1/0.91$. Note that since a negative/positive I_{d-v} represents excess/lack of energy in the network (that will increase/decrease ω_r), I_ω should be positive/negative for ω_r close to the max/min limit.

In order to improve the transient response of the virtual Governor and the AVR, a dynamic time-constant selection of the LPFs, illustrated in Fig.5, is proposed in this paper. The time-constant of the virtual Governor's LPF τ_f varies according to the absolute value of the frequency error $|f_{error}|$. Using the proposed methods, as $|f_{error}|$ increases, τ_f drops to reduce

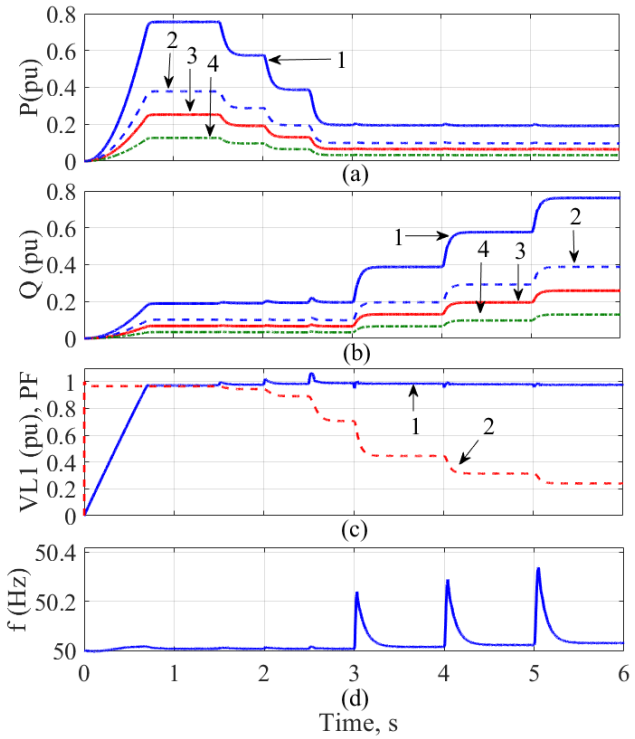

FIGURE 6. 20% Step changes in total load active and reactive power from very resistive (PF = 0.98) to very inductive (PF = 0.24), (a) active powers (pu), 1-$P_{L-total}$, 2-P_g, 3-P_1, 4-P_2, (b) reactive powers (pu), 1-$Q_{L-total}$, 2-Q_g, 3-Q_1, 4-Q_2, (c) 1-V_{L1} (pu), 2- PF seen by CBSs, (d) frequency at Load-1 (Hz).

the response time, while for small $|f_{error}|$ (at steady state), a higher τ_f provides more damping. The time-constant of the virtual AVR's LPF τ_v varies according to the magnitude of the inverter current $|I|$, which is imposed by the loads. Since at smaller loads oscillations increase, τ_v rises to increase damping. Reducing τ_v as current rises, also enables a fast and smooth black-start through establishing the voltage gradually (see Fig.6). The eigenvalue analysis explained in Appendix, shows that (1) the LPFs make the system more stable, (2) the dominant oscillatory modes become more stable as τ_f and τ_v increase (within their proposed range in Fig.5).

As shown in Fig.3, each unit has a synchronously referenced frame-phase locked loop (SRF-PLL) which imposes the nominal frequency ω_0. The PLLs also synchronize units through making their local q-component voltages $V_{C-q} = 0$. It is also noted that the nominal voltage value is imposed in the process of calculating the pu value of the local d-component voltages V_{C-d} (see Fig.3).

While the NSC of the SG is controlled using the proposed structure in Figs.3 & 4, the GSC, as shown in Fig.2, controls the DC-link voltage by regulating the SG-side active current I_d. The DC-link voltage controller is designed using the PI controller, based on the power balance principle (using cascaded voltage and current loops). The q-component of the GSC's current is set to zero in this paper; however, it can potentially be used (instead or alongside the AVR system) to control the SG's terminal voltage V_{sg}. Using the proposed structure/control, the SG's power P_{sg} (see Fig.2) is imposed (on the SG) by the NSC while the network operator can coordinate between units by adjusting I_{op} (Fig.1) according to the technical and economic criteria (not the subject of this paper). The ratings of the NSC and GSC must be at least equal to the rated apparent power of the SG in order to be able to provide the same active and reactive powers during normal operation. If the NSC is required to provide additional reactive power support, that must be considered in the rating of the NSC.

A simple Governor control is proposed to regulate the SG's prime mover (Fig.2). The control valve (CV) of the prime mover (e.g. a steam turbine) can vary from fully closed i.e. 0 to fully open i.e. 1. This value, at steady state, is equal to P_{sg} (neglecting losses) in $\text{pu}_{-\text{unit}}$ (i.e. based on SG's rating). A proportional controller (k_ω) is used to maintain the rotor speed ω_r transient response. A PI controller is not used as it is no longer needed to keep ω_r at 1 pu (50 or 60 Hz) at steady state, which enhances the ES capability of the SG.

The advantages of the proposed structure/control are:

1) Since all sources are connected through PECs, they will have similar SCL contribution; hence, the overcurrent relays can be accordingly set (i.e. no need to change it as the generation portfolio changes).
2) Since the SGs are physically separated from the network by PECs, they are protected against phase angle changes (see Fig.9).
3) Since the electrical and mechanical frequency are decoupled, RoCoF-based protection can be further relaxed or even removed. Note that in this structure the so-called islanded and grid-connected modes are merged (hence, no need to an islanding detection).
4) The proposed control method still allows the full utilization of the SGs' inertial capacity despite being physically disconnected from the network (see Figs.7, 9, 10, 12, & 14).
5) The proposed control method enables using SGs as ES systems (see Figs.7 & 14). Note that even a small amount of ES facilities in a network with a high penetration of renewable energy can play a crucial role.
6) Each segment of the network can seamlessly control the local voltage and frequency and supply the critical) loads (see Fig.10).
7) The control system works for both inductive and resistive loads (see Fig.6).

In addition to the above advantages, the proposed structure can potentially have further advantages that require further investigations (not considered in this paper), e.g.:

1) Since inter-area oscillations are mainly due to the slow electromechanical interaction of SGs, decoupling them from the network may disappear the inter-area oscillations.
2) It might be possible to use the PECs interfacing the SGs as "solid-state transformers" replacing the conventional ones (similar to the structure proposed in [36] for wind turbines).

TABLE 1. Systems parameters of Fig.2 (sub-sections *A-D*).

Parameter	Value
SG inertia, mechanical loss, k_ω	3.5 s, 0.005 pu, 3 pu
DC link Capacitance and Voltage of the SG's PEC	0.8 mF, and 20 kV
Transmission line	0.04+j0.319 Ω per km [37]
Transformers leakage reactance	3 %
PLLs' PI controller	K_p= 70, K_i=5
Z_{f1}, Z_{f2}, Z_{f3} (L_f =5% of $L_{base\text{-unit}}$)	$0.5e^{-3}$+j0.06, $0.5e^{-3}$+j0.1, $0.5e^{-3}$+j0.04 Ω
C_{f1}, C_{f2}, C_{f3} (2% of $C_{base\text{-unit}}$)	$5.26e^{-5}$, $2.63e^{-5}$, $7.9e^{-5}$ F

3) It might be possible to use the reactive power capacity of the SG's GSC to replace its AVR.

III. SIMULATION RESULTS

For sub-sections *A-D*, the system shown in Fig.2 is simulated. To avoid confusion with an energy management proposal, in sub-sections *A-D*, the CBSs are connected to DC voltage sources (see Fig.2), while I_{op} (the output of the EMS) is chosen according to different simulation scenarios. Sub-section *E* simulates system shown in Fig. 13, which includes a PV system fed by measured solar irradiation. Both systems are simulated using PSCAD/EMTDC. The PSCAD "IEEE Type Thermal Turbine" is used to model the prime mover, and the PSCAD "IEEE type SCRX solid-state exciter" is used to model the AVR.

The system shown in Fig. 2, consists of the aggregated models [12] of a 150 MVA SG and two CBSs (100 MVA and 50 MVA). The CBSs and the SG, through 5 km transmission lines, feed two sets of variable loads (each of maximum 150 MVA), while a 10 km transmission line connects the two sections. The system parameters are explained in Figs.2-5 and Table 1 (for sub - sections *A - D*). All simulation results (for sub-sections *A-D*) are shown in pu with base power of 300 MVA (total system rating). Different scenarios are simulated:

A. STEP CHANGES IN LOAD (VARYING FROM PF = 0.98 TO PF = 0.24)

The main purpose of this section is to demonstrate that the proposed control scheme can maintain voltage and frequency while the loads vary from very resistive to very inductive in large step changes. As shown in Fig.6, the total load active power $P_{L-total} = P_{L1} + P_{L2}$ (Fig.6(a)1) reduces from 0.8 pu to 0.2 pu (in 0.2 pu steps) while the total load reactive power $Q_{L-total} = Q_{L1} + Q_{L2} = 0.2$ pu (Fig.6(b)1). Then $Q_{L-total}$ increases to 0.8 pu (in 0.2 pu steps) while $P_{L-total} = 0.2$ pu. Fig.6(c)2 shows that the power factor (PF) reduces from 0.98 to 0.24 while both voltage (Fig.6(c)1) and frequency (Fig.6(d)) are well controlled. It is noted that while a "3-5% load change is considered to be a large disturbance to power systems" [38], the load change in this scenario is 20%. The PF is measured at CBSs terminal (i.e. P_{DG} and Q_{DG} in Fig.2). Although only voltage and frequency of Load-1 are shown, these are identical to those of Load-2. Fig.6 also demonstrates that it takes less than 1 s to establish the voltage and frequency from a black-start. It also shows that the method works for both inductive and resistive networks. It can be shown that the proposed method works just as well for capacitive loads, which is not considered in this paper. Fig.6(a)2-4 and Fig.6(b)2-4 also show that if the input power to all units is the same (i.e. the same I_{op}), active and reactive power will be shared proportional to the units' ratings.

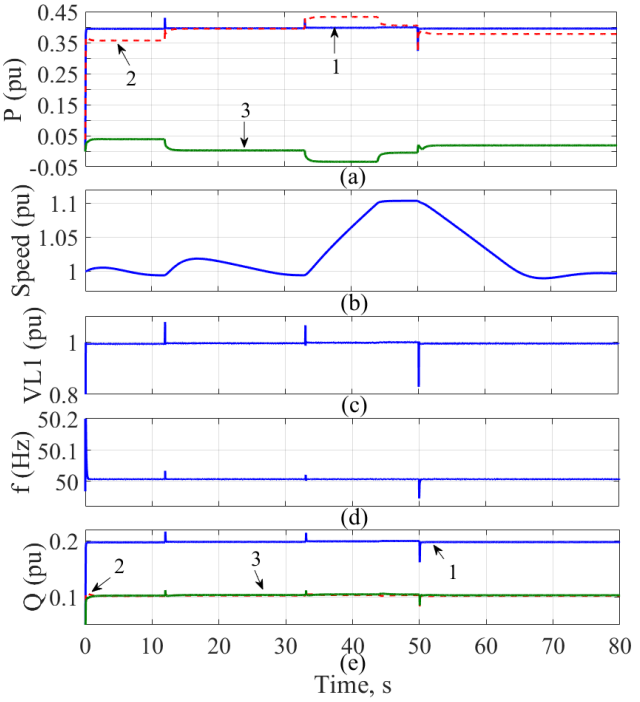

FIGURE 7. Variable power from CBSs, (a) active powers (pu), 1-$P_{L-total}$, 2-P_{DG}, 3-P_g, (b) SG rotor speed (pu), (c) V_{L1} (pu), (d) frequency at Load-1 (Hz), (e) reactive powers (pu), 1-$Q_{L=total}$, 2-Q_{DG}, 3-Q_g.

B. VARYING INPUT POWER (I_{op})

In the previous sub-section in order to focus on the applicability of the method to all types of load, it was assumed that the input power to the CBSs is the same as the SG (the same I_{op}), which made the sharing proportional to the units' ratings. In this sub-section the input power of CBSs varies by changing their I_{op}, which represent a varying renewable input. The simulation results are shown in Fig.7. As shown in Fig.7(a)1, $P_{L-total} = 0.4$ pu while initially the total power from the CBSs (Fig.7(a)2) $P_{DG} = P_1 + P_2 = 0.35$ pu. This is done by setting the I_{op} of each CBS unit to 0.7 $\text{pu}_{-\text{unit}}$, where $\text{pu}_{-\text{unit}}$ is defined as the pu value based on each unit rating (rather than the total system rating). Therefore, only the remaining power is demanded from the SG (Fig.7(a)3). At t = 12s, I_{op} of each CBS raises to 0.8 $\text{pu}_{-\text{unit}}$, which increases P_{DG} to 0.4 pu = $P_{L-total}$. Thus, the power from SG, seamlessly, drops to zero. This mode of SG operation is similar to the floating mode or SC operation, where no active power is exchanged (obviously, some power is needed to cover the mechanical and electrical losses). At t = 33s, CBSs' $I_{op} = 0.95$ $\text{pu}_{-\text{unit}}$, which makes $P_{DG} > P_{L-total}$ (note that due the actions of virtual governors and virtual AVRs of the CBSs to maintain the local voltage

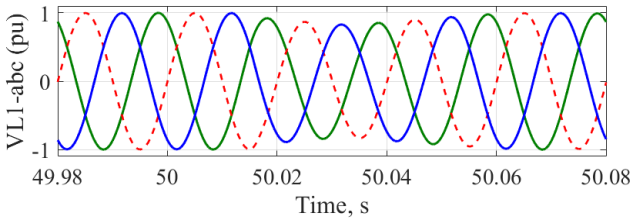

FIGURE 8. 3-phase V_{L1} (pu), zoomed-in at t = 50s of the scenario in Fig.7.

and frequency within acceptable limits, P_{DG} does not increase to $0.95/2 = 0.475$ pu). Since $P_{DG} > P_{L-total}$, a negative power is imposed on the SG (Fig.7(a)3), which means that the extra generated energy is stored in the rotor inertia of the SG, leading to an increase in its rotor speed (Fig.7(b)). As shown in Fig.7(b), the control structure of Fig.4 keeps the rotor speed within $\pm 10\%$. Fig.7 shows that when rotor speed hits the 1.1 pu limit, the CBSs power (Fig.7(a)2), seamlessly, reduces to $P_{L-total}$. Finally, at t = 50.01s, CBSs' $I_{op} = 0.75$ pu$_{-\text{unit}}$, which makes $P_{DG} < P_{L-total}$, leading to the release of the stored energy in rotor inertia and reduction in the rotor speed (Fig.7(b)). As can be seen, the Load-1 voltage V_{L1} (Fig.7(c)) and frequency (Fig.7(d)) are well controlled using the proposed control method (the same for V_{L2}). Fig.8, which shows the zoomed-in 3-phase voltage V_{L1}, demonstrates that the frequency and voltage are restored in less than 1 cycle and 2 cycles, respectively. Fig.7(e) shows that the load reactive power $Q_{L-total} = 0.2$ pu (Fig.7(e)1) is shared by the CBSs (Fig.7(e)2) and the SG's NSC (Fig.7(e)3) in proportion to their ratings. These results demonstrate that, despite physically decoupling the SGs from the network, the proposed control scheme still utilizes the SGs' inertial capacity and indeed enables further exploitation of their capacity as an ES mechanism (Fig.7(b)). This is simply because the rotor speed must no longer be synchronized to the network frequency. For example, from t = 33-65s (when $P_{DG} > P_{L-total}$), the rotor speed > 1 pu (50Hz) while the network frequency is maintained at 50 Hz.

C. DIFFERENT PHASE ANGLES

To demonstrate the performance of the proposed control structure when two sub-networks with different phase angles are connected, the circuit breakers (CBs) on the two sides of the 10 km lines (Fig.2) are initially open and will be closed at t = 1s while the loads on each side demand different reactive powers. The results are shown in Fig.9. Fig. 9 (a) illustrates that since $P_{L1} = P_{L2} = 0.15$ pu, the same active power is supplied by the CBSs (Fig.9(a)2), and the SG (Fig.9(a)3) i.e. before t = 1s, $P_{DG} = P_g = 0.15$ pu. However, while the load on the CBSs side (Load–1) demands $Q_{L1} = 0.1$ pu $= Q_{DG}$ (Fig.9(b)2), the load on the SG side (Load-2) demands $Q_{L2} = 0.45$ pu $= Q_g$ (Fig.9(b)3). Thus, as shown in Fig.9(e), which illustrates the phase-a of two load voltages right before the CBs closure, there is more than 120 degrees phase difference between V_{L1} and V_{L2}. Due to this large phase difference, as shown in Fig.9(d), the load voltages drop to almost 0.3 pu after closing the CBs. Fig.9(d), shows the

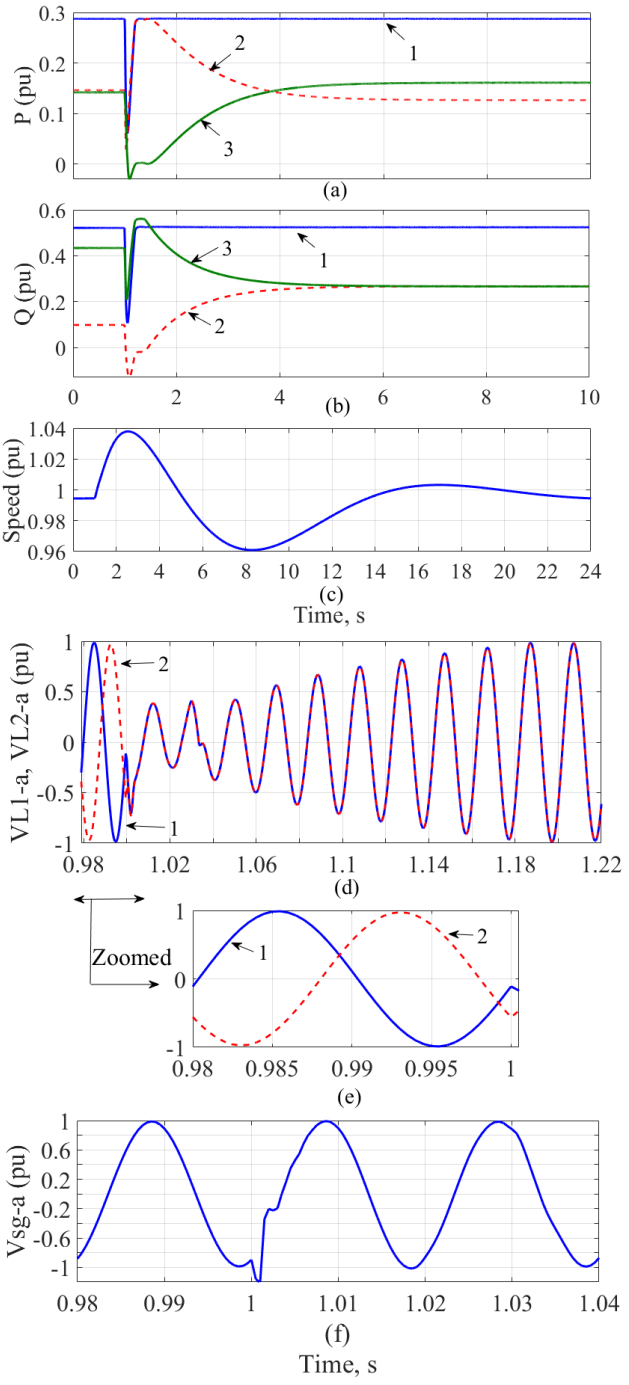

FIGURE 9. Connecting two sections with different phase angles, (a) active powers (pu), 1-$P_{L-total}$, 2- P_{DG}, 3-P_g, (b) reactive powers (pu), 1-$Q_{L-total}$, 2- Q_{DG}, 3-Q_g, (c) SG's rotor speed (pu), (d) Phase-a of the loads voltages (pu), 1-V_{L1-a}, 2-V_{L2-a}, (e) Zoomed in of (d) (pu), (f) Phase-a of the SG voltage V_{sg-a} (pu).

phase-a of V_{L1} and V_{L2}, illustrating that the voltages restore in less than 0.2s, and the frequency restores in less than 3 cycles. Fig.9(c) demonstrates that despite being physically decoupled, the SG still contributes to the system inertia and helps to suppress the disturbance, and the rotor speed is controlled by the proposed Governor. More importantly, it comes with the advantage of being immune from the phase difference,

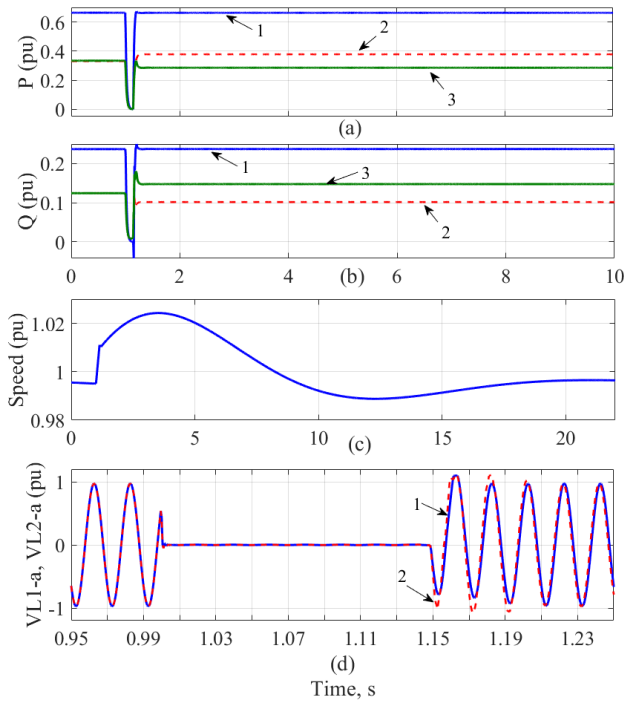

FIGURE 10. Separation of the two sections subsequent of a 3-phase fault at t = 1s, (a) active powers (pu), 1-$P_{L-total}$, 2- P_{DG}, 3-P_g, (b) reactive powers (pu), 1-$Q_{L-total}$, 2- Q_{DG}, 3-Q_g, (c) SG's rotor speed (pu), (d) Phase-a of the loads voltage (pu), 1-V_{L1-a}, 2-V_{L2-a}.

as shown in Fig.9(f), where no phase shift occurs in the SG terminal voltage V_{sg} (for the sake of clarity only phase-a of V_{sg} is shown).

D. FAULT RIDE-THROUGH

The performance of the proposed system for both symmetric and asymmetric faults is demonstrated in the following scenarios:

1) 3-PHASE FAULT; SEPARATION OF TWO SECTIONS

While $P_{L1} = 0.4$ pu, $P_{L2} = 0.3$ pu, $Q_{L1} = 0.1$ pu, and $Q_{L2} = 0.15$ pu, a 3-phase fault occurs in the middle of the 10 km line (Fig.2), and the protection system opens the two CBs after 150ms. The results are shown in Fig. 10. As per Figs. 10 (a) &(b), before the fault, the load is proportionally shared by the CBSs and the SG (Figs.10(a & b) 2,3). After the CBs removed the faulted area (i.e. the 10 km line) at t = 1.15s, each side of the network rides through the fault and takes over the load on its side. Note that this change is equivalent to $\Delta P = +/-0.1$ pu$_{-\text{unit}}$ and $\Delta Q = -/+0.05$ pu$_{-\text{unit}}$ variations for the CBSs/SG. Fig.10(c) shows that the SG's inertia contributes to suppress the disturbance while the proposed Governor controls the rotor speed. Fig.10(d), which illustrates the phase-a of the load voltages, shows that the voltage and frequency (of both sides) restore within 3 cycles. Figure 10 demonstrates that using the proposed control/structure each segment of the network can independently operate and supply the (critical) loads.

2) SINGLE PHASE TO GROUND FAULT

Although 3-phase faults are the most severe ones, they rarely occur. Since the most occurring faults are single-phase to ground one, this section considers it. To reduce the number of displayed results, some minor modifications, shown in Fig. 11, are applied on Fig. 2. Instead of the two loads, one load of the same total capacity is placed in the middle of the 10 km line, where a single-phase to ground fault occurs. The simulation results for this scenario are shown in Fig.12. As per Figs.12(a)&(b), $P_L = 0.8$ pu and $Q_L = 0.2$ pu are shared proportionally by the CBSs and the SG. The phase-a to ground fault occurs at t = 1s and after almost 150ms clears by itself (CBs remain closed). Figs.12(d)&(e) show that

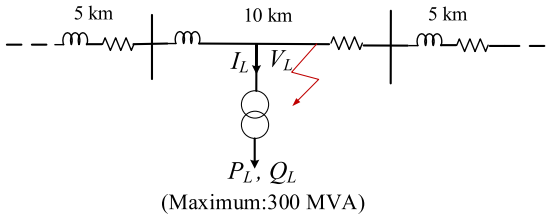

FIGURE 11. Modifications on Fig.2 to simulate sub-section *D*-2.

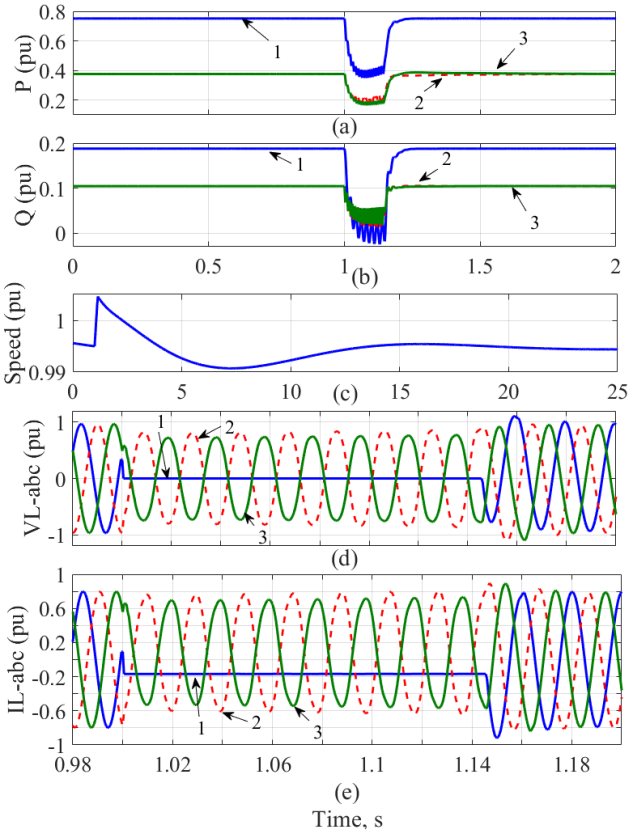

FIGURE 12. Phase-a to ground fault at t = 1s, (a) active powers (pu), 1-P_L, 2- P_{DG}, 3-P_g, (b) reactive powers (pu), 1-Q_L, 2- Q_{DG}, 3-Q_g, (c) SG's rotor speed (pu), (d) load voltage V_L (pu), 1-phase-a, 2-phase-b, 3-phase-c (e) load current I_L (pu), 1-phase-a, 2-phase-b, 3-phase-c.

TABLE 2. Systems parameters of Fig.13 (sub-section *E*).

Parameter	Value
DC link Capacitance of the SG's and PV system's PEC	3 μF
Z_f (L_f=5% of $L_{base\text{-unit}}$)	0.5e^{-3}+j1.2 Ω
C_f (2% of $C_{base\text{-unit}}$)	2.6 μF

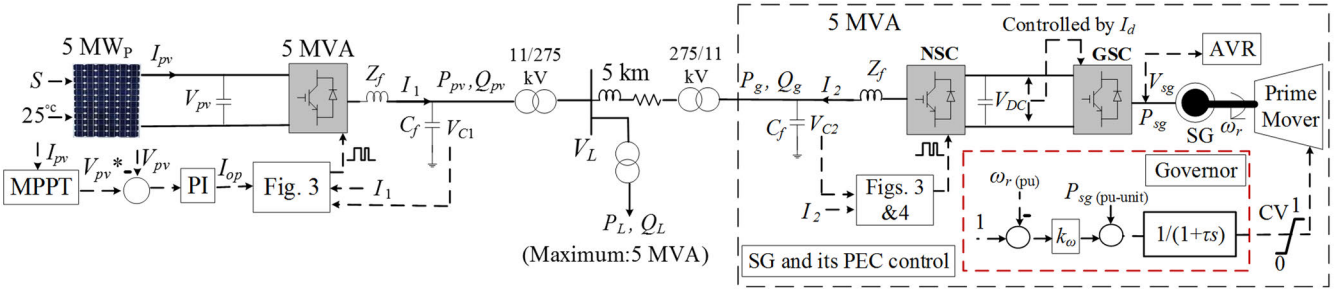

FIGURE 13. Simulated system for sub-section III-*E*.

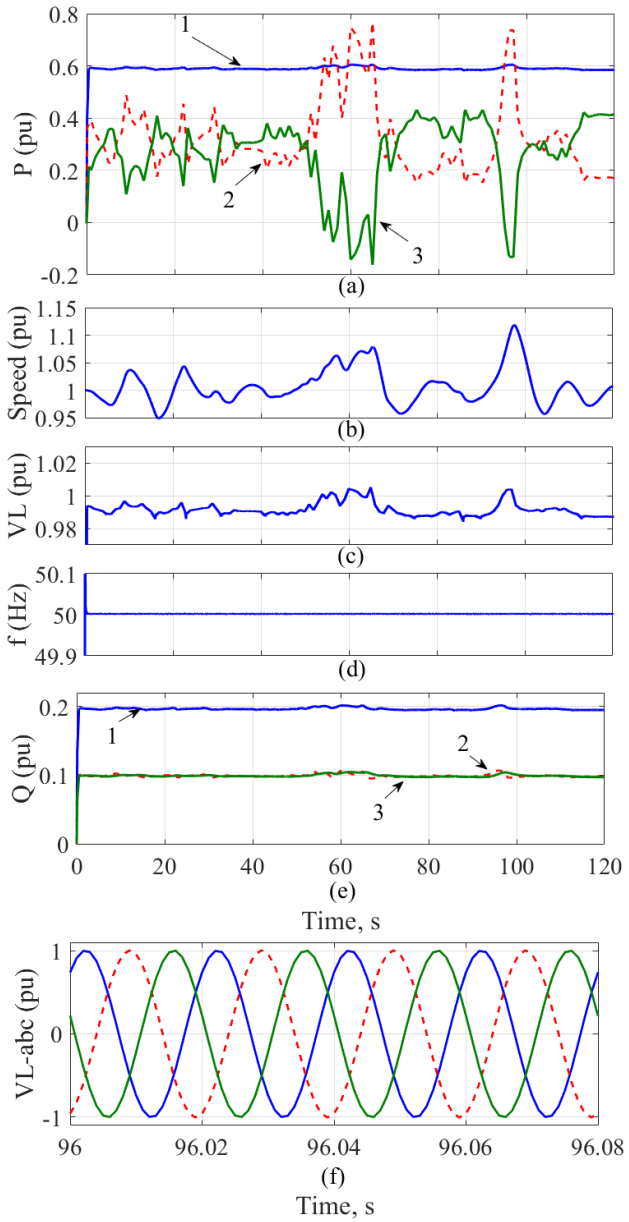

FIGURE 14. Simulated simulation results of Fig.13, (a) active powers (pu), 1-P_L, 2-P_{pv}, 3-P_g, (b) rotor speed (pu), (c) V_L (pu), (d) frequency (Hz), (e) reactive powers (pu), 1-Q_L, 2-Q_{pv}, 3-Q_g, (f) 3-phase load voltage V_L (pu).

during the fault, the voltage and current of the healthy phases (i.e. phase-b and phase-c) remain sinusoidal, which means that the loads connected to the healthy phases will not be affected. It can also be seen that the voltage and frequency restore within 3 cycles. Fig12(c) again demonstrates that the SG still contributes to the system inertia while the rotor speed is well controlled.

E. REAL SOLAR IRRADIATION SCENARIO

This sub-section simulates the system shown in Fig.13, which consists of a 5 MW_P PV array (controlled by a 5 MVA DC/AC converter) and a 5 MVA SG (and its PECs), which are sharing a load rated at 5 MVA. Fig.13 shows that the MPPT algorithm [39] sets the reference PV voltage V^*_{pv}, which is controlled by the voltage loop through regulating I_{op}, which is fed to the proposed control system in Fig.3. The solar irradiation S used in this simulation is measured at Swansea University's "Active Classroom" in August 2019. Table 2 shows the system parameters (those changed from Table 1). The simulation results are illustrated in Fig.14 for the based power of 5 MVA. As shown, $P_L = 0.6$ pu (Fig.14(a)1) and $Q_L = 0.2$ pu (Fig.14(e)1). As solar power P_{pv} (Fig. 14 (a) 2) varies, the power demanded from the SG P_g (Fig. 14 (a) 3), seamlessly, changes to keep P_L constant. Note that while there is no external ES system, the SG's inertia is operating as an ES mechanism to smooth out the solar irradiation, leading to its rotor speed variations (Fig.14(b)). To show that the ±10% speed variation limit in Fig. 4 was an arbitrary number (chosen only to demonstrate the method in Fig.7), a ±20% limit is applied in this sub-section, which led to the rotor speed increases more than 1.1 pu. The practical speed limit can differ for different designs of SG and is not the subject of this paper. Since the SG is physically decoupled from the network, despite the large rotor speed variations, the load frequency (Fig.14(d)) and voltage (Fig.14(c)) are well controlled. Fig.14(f) illustrates the zoomed-in 3-phase load voltage to demonstrate the accuracy of the measured frequency. Fig.14(e) shows that Q_L is shared by the PECs of the PV and the SG proportionally.

IV. CONCLUSION

The ever-increasing penetration of CBSs (e.g. renewable energy), has been causing numerous challenges for the network operators and has put the power networks on the verge of instability. Some of these challenges, which are due to the intermittent nature of renewable energy, do not depend on the power system structure. For example, as the penetration of renewable energy increases, more ES facilities will be needed regardless of the system structure. However, as discussed in

the Introduction, there are some challenges (such as reduction in the SCL, phase angle movement, and RoCoF) that do depend on the system structure. To alleviate these issues the popular approach is to make the CBSs behave like SGs. It was argued in the Introduction that this approach, which involves slowing down the dynamics of PECs and utilizing over-rated switches, is not optimized. This paper proposed a "steer into the skid" strategy involving the decoupling of SGs from the network using AC/DC/AC PECs and proposed a universal control structure that can be used for SGs, renewable energy, and ES systems in both inductive and resistive networks. It was shown that using the proposed structure and control scheme, the SGs' inertia, despite being physically decoupled from the network, will still be used to suppress the oscillations caused by disturbances. Moreover, the proposed method enables further exploitation of SGs' inertial capacity as an ES mechanism since the SGs' speed must no longer be synchronized to the network frequency. It was also shown that the proposed method works for all types of loads, rides-through both symmetric and asymmetric faults, and withstands large phase differences without affecting the SGs. The proposed structure will also remove the mechanical meaning of the network frequency from its electrical definition, which in turns creates room for new standards and regulations. Moreover, separating the slow dynamics of the SGs from the network enables faster control of voltage and frequency without affecting the SGs.

It is noted that the main extra costs associated to the proposed structure/control is the SG's PECs. Since the network operators are expected to invest millions on stability provider technologies (e.g. ES mechanisms), which are interfaced by PECs, the proposed structure/control appears financially justifiable (or at least considered against other approaches). For example, using the proposed method will exploit the SGs as ES systems, which means fewer extra ES + PEC mechanisms will be needed. Or, in addition to other advantages, the proposed structure/control saves the network operators from using over-rated (up to 5 pu) PECs to maintain the SCL, which will reduce the energy price. Although it appears that the proposed structure/control is financially justifiable, this paper does not claim that a Costs-Benefits Analysis is performed as it requires a case study (which is beyond the scope of this paper). The main aim is to initiate the discussion about this strategy within academic and industrial communities to further investigate its advantages and drawbacks.

APPENDIX

The test system for the eigenvalue analysis is an islanded 2.2 MVA CBS feeding a load through an LC filter ($L_f = 0.15$ mH, $R_f = 1.5$ mΩ, and $C_f = 160$ μF). The CBS, which is connected to a DC voltage source, is controlled using the proposed method in Fig.3 ($I_{op} = 0$) and feeds an RL load of $P_L = 0.8$ pu at PF = 0.9. The initial time-constant of the LPFs are $\tau_f = 0.3$ and $\tau_v = 0.5$. The complete state space model of the test system is developed in MATLAB/SIMULINK using the linear analysis toolbox. Table 3 illustrates the complete eigenvalues of the test system and the dominant states, which are derived using the participation factor analysis [1]. From Table 3, it is observed that the CBS is well-damped as all the modes have a damping ratio $\zeta > 0.05$ [40]. The modes $\lambda_{1,2}$ and $\lambda_{3,4}$, which are oscillating close to the nominal frequency, are dominated by the filter capacitor voltage V_C, LPFs and the load. The sub-synchronous oscillatory modes $\lambda_{5,6}$ are dominated by L_f and load, while $\lambda_{7,8}$ are dominated by the PLL and LPFs. The non-oscillatory modes λ_9, λ_{10} and λ_{11} are dominated by the PLL, LPFs and the current controllers. To investigate the impact of the LPFs on the system stability, three test scenarios are investigated: (a) comparing the stability of the CBS with and without the LPFs (b) impact of varying τ_v (c) impact of varying τ_f.

TABLE 3. Complete system eigenvalues.

Eigenvalues (λ)	Damping ratio (ζ)	f (Hz)	Dominant states/parameters
$\lambda_{1,2}$= -5.7e4±j318	1	50.61	$V_{C\text{-}d}$, $V_{C\text{-}q}$
$\lambda_{3,4}$= -76±j284	0.26	45.20	Load, τ_f, τ_v
$\lambda_{5,6}$= -1.4e3±j13	1	2.07	Load, L_f
$\lambda_{7,8}$= -37±j12	0.95	1.91	τ_f, τ_v, PLL
λ_9= -17	1		PLL, τ_f, i_q
λ_{10}= -8.35	1		PLL, i_q
λ_{11}= -11.6	1		i_d, τ_v

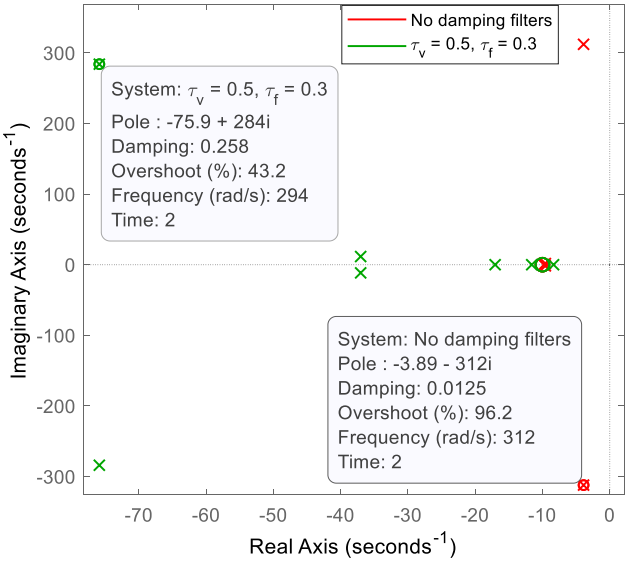

FIGURE 15. Impacts of the LPFs on the stability of the CBS.

A. STABILITY WITH AND WITHOUT LPFs

Figure 15 compares the poles of the CBS with and without the LPFs. As illustrated in Fig.15, without the LPFs the oscillatory poles $\lambda_{3,4}$ are situated very close to the $j\omega$-axis, indicating a poorly damped system ($\zeta = 0.0125$). However, with the inclusion of the LPFs ($\tau_f = 0.3$ and $\tau_v = 0.5$) the oscillatory poles $\lambda_{3,4}$ moves towards the left-hand side (LHS) indicating a well-damped system ($\zeta = 0.258$) with improved stability.

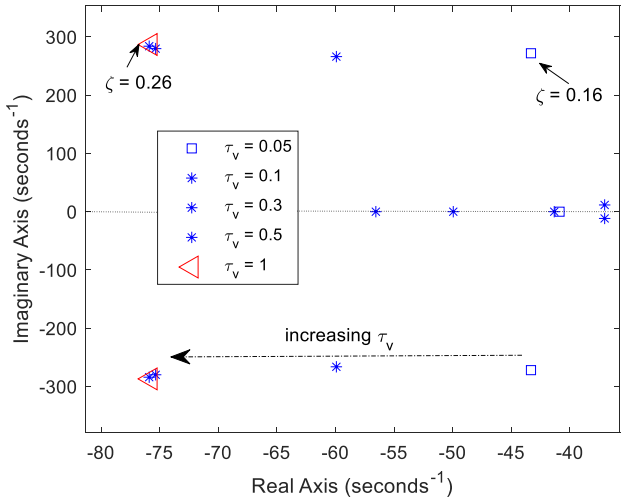

FIGURE 16. Impacts of varying τ_v from 0.05 to 1 while $\tau_f = 0.3$.

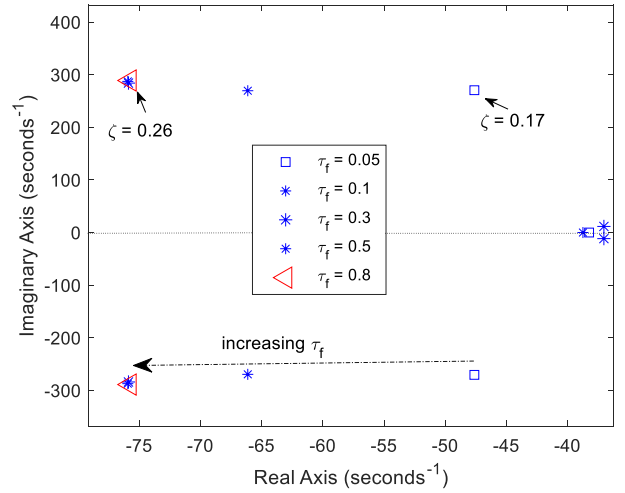

FIGURE 17. Impacts of varying τ_f from 0.05 to 0.8 while $\tau_v = 0.5$.

B. IMPACT OF VARYING τ_v

The impact of the virtual AVR damping LPF τ_v on the CBS stability is observed by maintaining τ_f at 0.3 while τ_v is varied from 0.05 to 1 (according to Fig. 5). From Fig. 16, it is observed that by increasing τ_v, the oscillatory poles $\lambda_{3,4}$ move further to the LHS of the $j\omega$-axis, indicating improved stability and damping. As illustrated in Fig. 16, ζ of $\lambda_{3,4}$ increases from 0.16 to 0.26, as τ_v varies from 0.05 to 1.

C. IMPACT OF VARYING τ_f

The impact of the virtual governor LPF τ_f on the CBS stability is observed by maintaining τ_v at 0.5 while τ_f is varied from 0.05 to 0.8 (according to Fig. 5). From Fig.17, it is observed that by increasing τ_f, the oscillatory poles $\lambda_{3,4}$ move further to the LHS of the $j\omega$-axis, indicating improved stability and damping. Also, as τ_f is increased from 0.05 to 0.8, ζ increases from 0.17 to 0.26.

The eigenvalue analysis demonstrates that that (1) the LPFs make the system more stable, (2) the dominant oscillatory modes become more stable as τ_f and τ_v increase (within their proposed range in Fig.5).

REFERENCES

[1] P. Kundur, *Power Systems Stability and Control* (The EPRI Power System Engineering Series). New York, NY, USA: McGraw-Hill, 1994.
[2] I. Sadeghkhani, M. E. H. Golshan, J. M. Guerrero, and A. Mehrizi-Sani, "A current limiting strategy to improve fault ride-through of inverter interfaced autonomous microgrids," *IEEE Trans. Smart Grid*, vol. 8, no. 5, pp. 2138–2147, Sep. 2017.
[3] N. Etherden, V. Vyatkin, and M. H. J. Bollen, "Virtual power plant for grid services using IEC 61850," *IEEE Trans. Ind. Informat.*, vol. 12, no. 1, pp. 447–473, Feb. 2016.
[4] A. Baringo, L. Baringo, and J. M. Arroyo, "Day-ahead self-scheduling of a virtual power plant in energy and reserve electricity markets under uncertainty," *IEEE Trans. Power Syst.*, vol. 34, no. 3, pp. 1881–1894, May 2019.
[5] S. L. Arun and M. P. Selvan, "Intelligent residential energy management system for dynamic demand response in smart buildings," *IEEE Syst. J.*, vol. 12, no. 2, pp. 1329–1340, Jun. 2018.
[6] P. Babahajiani, Q. Shafiee, and H. Bevrani, "Intelligent demand response contribution in frequency control of multi-area power systems," *IEEE Trans. Smart Grid*, vol. 9, no. 2, pp. 1282–1291, Mar. 2018.
[7] J. Rocabert, A. Luna, F. Blaabjerg, and P. Rodríguez, "Control of power converters in AC microgrids," *IEEE Trans. Power Electron.*, vol. 27, no. 11, pp. 4734–4749, Nov. 2012.
[8] F. Milano, F. Dörfler, G. Hug, D. J. Hill, and G. Verbič, "Foundations and challenges of low-inertia systems," presented at the Power Syst. Comput. Conf., Dublin, Republic of Ireland, Jun. 2018.
[9] *The Telegraph*. Accessed: Sep. 9, 2019. [Online]. Available: https://www.telegraph.co.uk/politics/2019/08/18/former-national-grid-director-says-ministers-shouldimpose-limits/?WT.mc_id=tmgliveapp_androidshare_As67sdG4xwcT
[10] *Stability Pathfinder*. National Grid ESO, Warwik, UK. Accessed: Sep. 4, 2019. [Online]. Available: https://www.nationalgrideso.com/news/carbon-free-system-stability-pathfinder-stakeholder-feedback-request
[11] *System Operability Framework*. National Grid ESO, Warwik, UK. Accessed: Sep. 4, 2019. [Online]. Available: https://www.nationalgrideso.com/document/63476/download
[12] J. Zhu, J. Hu, W. Hung, C. Wang, X. Zhang, S. Bu, Q. Li, H. Urdal, and C. D. Booth, "Synthetic inertia control strategy for doubly fed induction generator wind turbine generators using lithium-ion supercapacitors," *IEEE Trans. Energy Convers.*, vol. 33, no. 2, pp. 773–783, Jun. 2018.
[13] W. Winter, K. Elkington, G. Bareux, and J. Kostevc, "Pushing the limits: Europe's new grid: Innovative tools to combat transmission bottlenecks and reduced inertia," *IEEE Power Energy Mag.*, vol. 13, no. 1, pp. 60–74, Jan. 2015.
[14] *Network Code on Operational Security*. ENSTO-e. Accessed: Sep. 4, 2019. [Online]. Available: https://www.entsoe.eu/fileadmin/user_upload/_library/resources/OS_NC/130227-AS-NC_OS_final_.pdf
[15] M. F. M Arani and E. F. El-Saadany, "Implementing virtual inertia in DFIG-based wind power generation," *IEEE Trans. Power Syst.*, vol. 28, no. 2, pp. 1373–1384, May 2013.
[16] L. He, Y. Li, J. M. Guerrero, and Y. Cao, "A comprehensive inertial control strategy for hybrid AC/DC microgrid with distributed generations," *IEEE Trans. Smart Grid*, vol. 11, no. 2, pp. 1737–1747, Mar. 2020.
[17] M. Karimi-Ghartemani, "Universal integrated synchronization and control for single-phase DC/AC converters," *IEEE Trans. Power Electron.*, vol. 30, no. 3, pp. 1544–1557, Mar. 2015.
[18] S. Wang, J. Hu, X. Yuan, and L. Sun, "On inertial dynamics of virtual-synchronous-controlled DFIG-based wind turbines," *IEEE Trans. Energy Convers.*, vol. 30, no. 4, pp. 1691–1702, Dec. 2015.
[19] H. Wu, X. Ruan, D. Yang, X. Chen, W. Zhao, Z. Lv, and Q.-C. Zhong, "Small-signal modeling and parameters design for virtual synchronous generators," *IEEE Trans. Ind. Electron.*, vol. 63, no. 7, pp. 4292–4303, Jul. 2016.
[20] Q.-C. Zhong and G. Weiss, "Synchronverters: Inverters that mimic synchronous generators," *IEEE Trans. Ind. Electron.*, vol. 58, no. 4, pp. 1259–1267, Apr. 2011.
[21] A. S. Ahmadyar, S. Riaz, G. Verbic, A. Chapman, and D. J. Hill, "A framework for assessing renewable integration limits with respect to frequency performance," *IEEE Trans. Power Syst.*, vol. 33, no. 4, pp. 4444–4453, Jul. 2018.

[22] S. Teimourzadeh, F. Aminifar, M. Davarpanah, and J. M. Guerrero, ''Macroprotections for microgrids: Toward a new protection paradigm subsequent to distributed energy resource integration,'' *IEEE Ind. Electron. Mag.*, vol. 10, no. 3, pp. 6–18, Sep. 2016.
[23] H. Wen and M. Fazeli, ''A low-voltage ride-through strategy using mixed potential function for three-phase grid-connected PV systems,'' *Electric Power Syst. Res.*, vol. 173, pp. 271–280, Aug. 2019.
[24] J. Quintero, V. Vittal, G. T. Heydt, and H. Zhang, ''The impact of increased penetration of converter control-based generators on power system modes of oscillation,'' *IEEE Trans. Power Syst.*, vol. 29, no. 5, pp. 2248–2256, Sep. 2014.
[25] M. Garmroodi, D. J. Hill, G. Verbic, and J. Ma, ''Impact of tie-line power on inter-area modes with increased penetration of wind power,'' *IEEE Trans. Power Syst.*, vol. 31, no. 4, pp. 3051–3059, Jul. 2016.
[26] X. Jin, C. Bai, Z. Zhang, S. Zhao, H. Wang, Z. Yan, L. Zhang, and S. Chen, ''Blockchain-enabled transactive method in distributed systems considering security constraints,'' presented at the IEEE Congr. Evol. Comput. (CEC), 2019.
[27] A. M. Jadhav, N. R. Patne, and J. M. Guerrero, ''A novel approach to neighborhood fair energy trading in a distribution network of multiple microgrid clusters,'' *IEEE Trans. Ind. Electron.*, vol. 66, no. 2, pp. 1520–1531, Feb. 2019.
[28] M. Fazeli and P. Holland, ''Universal and seamless control of distributed resources-energy storage for all operational scenarios of microgrids,'' *IEEE Trans. Energy Convers.*, vol. 32, no. 3, pp. 963–973, Sep. 2017.
[29] Q.-C. Zhong, ''Power-electronics-enabled autonomous power systems: Architecture and technical routes,'' *IEEE Trans. Ind. Electron.*, vol. 64, no. 7, pp. 5907–5918, Jul. 2017.
[30] M. Hirst, ''Energy distribution microgrid in control, operation, management and power quality within a 100% converter, zero-inertia microgrid,'' presented at the 17th Wind Integr. Workshop, Stockholm, Sweden, Oct. 2018, pp. 17–19.
[31] S. Shrivastava, B. Subudhi, and S. Das, ''Consensus-based voltage and frequency restoration scheme for inertia-less islanded microgrid with communication latency,'' presented at the IEEE Region Conf. (TENCON), Malaysia, India, 2017.
[32] L. R. Castillo and A. Roscoe, ''Experimental validation of a novel inertia-less VSM algorithm,'' in *Proc. IEEE Power Energy Soc. Innov. Smart Grid Technol. Conf. (ISGT)*, Feb. 2018, pp. 1–5.
[33] M. Yu, A. J. Roscoe, R. Ierna, and H. Urdal, ''Use of an inertia-less virtual synchronous machine within future power networks with high penetrations of converters,'' presented at the IEEE Power Syst. Comput. Conf. (PSCC), 2016.
[34] M. O. Baruwa, M. Fazeli, and A. M. Egwebe, ''New control paradigm for both islanded and grid-connected operation of PMSG-based wind turbine,'' *J. Eng.*, vol. 2019, no. 18, pp. 5142–5146, Jul. 2019.
[35] Q.-C. Zhong and Y. Zeng, ''Universal droop control of inverters with different types of output impedance,'' *IEEE Access*, vol. 4, pp. 702–712, 2016.
[36] I. Syed and V. Khadkikar, ''Replacing the grid interface transformer in wind energy conversion system with solid-state transformer,'' *IEEE Trans. Power Syst.*, vol. 32, no. 3, pp. 2152–2160, May 2017.
[37] B. M. Weedy, B. J. Cory, N. Jenkins, J. B. Ekanayake, and G. Strbac, *Electric Power Systems*, 5th ed. Wiley, 2013.
[38] J. Fang, H. Li, Y. Tang, and F. Blaabjerg, ''On the inertia of future more-electronics power systems,'' *IEEE J. Emerg. Sel. Topics Power Electron.*, vol. 7, no. 4, pp. 2130–2146, Dec. 2019.
[39] M. Fazeli, P. Igic, P. M. Holland, R. P. Lewis, and Z. Zhou, ''Novel maximum power point tracking with classical cascaded voltage and current loops for photovoltaic systems,'' presented at the IET Conf. Renew. Power Gener. RPG, Edinburgh, U.K., 2011.
[40] O. Kotb, M. Ghandhari, R. Eriksson, and V. K. Sood, ''On small signal stability of an AC/DC power system with a hybrid MTDC network,'' *Electr. Power Syst. Res.*, vol. 136, pp. 79–88, Jul. 2016.

MEGHDAD FAZELI (Senior Member, IEEE) received the M.Sc. and Ph.D. degrees from Nottingham University, U.K., in 2006 and 2011, respectively.

From 2011 to 2012, he was a Research Assistant with Swansea University recruited on the ERDF-Funded Project of Solar Photovoltaic Academic Research Consortium (SPARC), where he worked on integration of large PV systems, aimed to provide ancillary services. In 2013, he has worked as a Research Officer with Swansea University on the Smart Operation for Low Carbon Energy Region (SOLCER) Project for a couple of months. In September 2013, he became an Academic Staff with the College of Engineering, Swansea University, where he is currently a Senior Lecturer. His main research interests include integration and control of renewable energy, ancillary services, VSMs, using AIs in forecasting algorithms, and microgrids.

PAUL M. HOLLAND (Member, IEEE) received the B.Sc. degree (Hons.) in engineering physics from Sheffield Hallam University, U.K., in 1993, and the Ph.D. degree in electrical and electronic engineering from Swansea University, U.K., in 2007.

He spent the first ten years of his career working in the semiconductor industry in senior process and device engineering Research and Development roles, U.K. He was appointed as the Dean of educational technology with Swansea University, between 2017 and 2019. He currently leads a Group of 20 Academic Staff in the Learning and Teaching Excellence Centre (LTEC), College of Engineering, Swansea University. He has over 50 publications and several patents and has been funded by sources, including EPSRC, Industry, ERDF, HEFCW, and the Wolfson Foundation. His research interests include power systems, power electronics, and CMOS-based medical devices. His academic research interests include leadership for excellence in learning and teaching.

MUFTAU BARUWA received the B.Eng. degree (Hons.) in electrical and electronic engineering from the University of Ilorin, Kwara, Nigeria, in 2012, and the M.Sc. degree (Hons.) in electrical and electronic engineering from Swansea University, U.K., in 2015, where he is currently pursuing the Ph.D. degree in electrical and electronic engineering.

His current research interests include the integration of renewable energy systems, design and control of virtual synchronous machine-based energy systems, and multi-machine stability analysis.